Journal of Petroleum Science and Engineering xxx (xxxx) xxx

Contents lists available at ScienceDirect

Journal of Petroleum Science and Engineering

journal homepage: http://www.elsevier.com/locate/petrol

Analytical solutions for forced and spontaneous imbibition accounting for viscous coupling

Pål Østebø Andersen [a,b,c,*], Eirik K. Nesvik [a], Dag C. Standnes [a]

[a] Department of Energy Resources, University of Stavanger, 4036 Stavanger, Norway
[b] Department of Energy and Petroleum Engineering, University of Stavanger, 4036 Stavanger, Norway
[c] The National IOR Centre of Norway, University of Stavanger, 4036 Stavanger, Norway

ARTICLE INFO

Keywords:
Viscous coupling interactions
Spontaneous imbibition
Forced imbibition
Capillary forces
Universal time scale

ABSTRACT

Fluid-fluid momentum transfer can cause higher flow resistance when fluids flow in opposite directions as compared to the same direction. Conventional modelling of flow in porous media using simple, saturation dependent relative permeabilities does not account for such variations.

We consider a generalized theory for multiphase flow in porous media based on mixture theory, where fluid mobilities follow from water-rock, oil-rock and water-oil interaction terms defined in momentum equations. Under strictly co- or counter-current flow modes, the generalized model produces explicit relative permeability expressions dependent on the flow mode, saturations, viscosities and interaction parameters. New expressions for counter-current relative permeabilities are derived assuming zero net flux, representative of counter-current spontaneous imbibition. These functions are compared to previously derived co-current relative permeabilities (assuming equal phase pressure gradients). The functions are incorporated into analytical solutions for forced and spontaneous imbibition (FI and SI) using the theory by Buckley and Leverett (1942) and McWhorter and Sunada (1990), respectively.

Our results show that when accounting for viscous coupling; Counter-current relative permeabilities are always lower than co-current ones, including the end points. Both phase curves are reduced by the same saturation dependent coefficient. Increased viscous coupling in the FI case led to a more effective displacement, seen as an increased front saturation and average water saturation behind the front. For counter-current SI, increased viscous coupling resulted in lower imbibition rate. Increased viscosities reduces both oil and water counter-current relative permeabilities, and predict greater reduction in imbibition rate than only modifying the viscosities. The analytical solutions for SI were in agreement with numerical solutions of both a conventional and generalized model. The solutions for SI could be scaled exactly to a square root of time curve for arbitrary input parameters in the generalized model, especially including the strength of viscous coupling.

1. Introduction

Darcy's law (Darcy, 1856) for flow in porous media was extended to two-phase flow by Muskat et al. (1937) by introducing relative permeabilities. The common assumption is that the relative permeability is a function of saturation only. Consequently, this standard approach does not account for the role of fluid-fluid interactions between the flowing phases, referred to as viscous coupling. Theory and experimental observations indicate that fluids travelling in opposite directions (counter-currently) experience greater flow resistance and hence lower mobilities compared to when they both travel in the same direction (co-currently) (Babchin et al., 1998; Bentsen and Manai, 1992; Bourbiaux and Kalaydjian, 1990; Dullien and Dong, 1996). Similar phenomena are induced by variations in fluid velocities and viscosities (Armstrong et al., 2017; Ehrlich, 1993; Wang et al., 2006; Odeh, 1959; Nejad et al., 2011). The relative permeabilities measured in the laboratory are typically from unsteady state or steady state tests. Both setups represent co-current displacements (Geffen et al., 1951; Richardson et al., 1952; Bear, 2013) where either just water or both water and oil are injected from one side of a core and both phases are produced at the other. Due to the mentioned phenomena, the resulting functions may not transfer directly to counter-current flow settings. Bourbiaux and

* Corresponding author. Department of Energy Resources, University of Stavanger, 4036 Stavanger, Norway.
E-mail address: pal.andersen@uis.no (P.Ø. Andersen).

https://doi.org/10.1016/j.petrol.2019.106717
Received 29 July 2019; Received in revised form 5 November 2019; Accepted 17 November 2019
Available online 22 November 2019

Kalaydjian (1990) found that predicting counter-current oil recovery using relative permeabilities determined in a co-current setting led to overestimation of both recovery rate and ultimate oil recovery. Other researchers have demonstrated similar results (Pooladi-Darvish and Firoozabadi, 1998; 2000; Standnes, 2004; Karimaie et al., 2006). This is particularly relevant when scaling up laboratory results for prediction of oil recovery from naturally fractured reservoirs, where both co- and counter-current spontaneous imbibition can be important recovery mechanisms (Pooladi-Darvish and Firoozabadi, 2000; Mason and Morrow, 2013; Andersen, 2019). While there is substantial evidence indicating that multiphase flow modelling is more complex than proposed by the simple saturation dependent relative permeability, there is still no agreed upon method of predicting relative permeabilities if the flow mode is changed.

In this work, the generalized model for multiphase flow based on mixture theory derived previously in Standnes et al. (2017); Qiao et al. (2018); Andersen et al. (2019a) will be studied. The model gives fluid mobilities that depend on water-rock, oil-rock and water-oil interaction terms, defined from momentum equations. Assuming either strictly co- or counter-current flow modes, the generalized model gives rise to flow mode dependent relative permeability expressions. Such expressions have been derived under the assumption of equal magnitude pressure gradients with same or opposite direction, respectively, in the stated works. Novel to this work, we will derive counter-current relative permeabilities under the assumption of equal, but oppositely directed *fluxes*, which is commonly taken representative of SI with all open sides exposed to wetting phase Mason and Morrow (2013). These curves will be compared to the mentioned co-current relative permeability functions based on equal pressure gradients taken representative of standard measurement procedures. These generalized relative permeabilities are implemented into analytical solutions for co-current forced imbibition as described by Buckley and Leverett (1942) and counter-current spontaneous imbibition as described by McWhorter and Sunada (1990); Schmid and Geiger (2012), thus extending previous analytical solutions to account for viscous coupling. It is noted that the analytical solution for counter-current SI assumes a semi-infinite medium and hence comparison with a numerical model with closed inner boundary is made. The numerical model is based on generalized formulation and is hence also used to validate the assumption of a relative permeability formulation for that flow regime. Numerical examples are included to demonstrate the role of viscous coupling terms on relative permeability functions and flow. Finally, we show that the analytical solution which previously has been shown to scale SI under arbitrary combinations of standard relative permeability and capillary pressure functions also can be extended to scale viscous coupling by means of the generalized relative permeabilities.

2. Theory

2.1. Derivation of generalized model from mixture theory

In this section we briefly derive the generalized model along the same lines as previously presented in Qiao et al. (2018); Andersen et al. (2019a).

2.1.1. Transport equations

1D mass balance equations for horizontal, incompressible transport of water (w) and oil (o) are given by:

$$\varphi \frac{\partial s_i}{\partial t} + \frac{\partial u_i}{\partial x} = 0, \qquad (i = w, o) \tag{1}$$

and the following equation expresses the relation between Darcy flux and interstitial velocity in the mobile domain:

$$u_i = \varphi (s_i - s_{ir}) v_i, \tag{2}$$

φ is porosity, s_i fluid saturation, s_{ir} residual fluid saturation and v_i is interstitial fluid velocity. By introducing effective porosity φ_e and normalized saturation S_i:

$$\varphi_e = \varphi(1 - s_{or} - s_{wr}), \qquad S_i = \frac{s_i - s_{ir}}{1 - s_{or} - s_{wr}}, \qquad (i = w, o), \tag{3}$$

the velocity relation 2 can be reformulated to:

$$u_i = \varphi_e S_i v_i, \qquad (i = w, o). \tag{4}$$

The saturations must add to unity due to conservation of volume and the phase pressures are assumed related by the imbibition capillary pressure function:

$$s_w + s_o = 1, \qquad p_o - p_w = p_c(s_w). \tag{5}$$

These equations are so far in line with conventional modelling. What separates the generalized model from the approach based on Darcy's law is the relations between fluxes and pressure gradients.

Ignoring inertial effects, as is usual for creeping (slow) flow in porous media, the mechanical stress balance for a fluid is given by (Ambrosi and Preziosi, 2002):

$$\frac{\partial (S_i \sigma_i)}{\partial x} + m_i = 0, \qquad (i = w, o), \tag{6}$$

where σ_i represents the Cauchy stress tensor and m_i represents interaction forces exerted on fluid i by the other constituents of the mixture. In 1D, the standard expression for the stress term is:

$$\sigma_i = -p_i + \tau_i, \qquad (i = w, o), \tag{7}$$

where τ_i represents viscous stress. The contribution from τ_i is ignored ($\tau_i = 0$). The interaction forces m_i are given by (Preziosi and Farina, 2002; Ambrosi and Preziosi, 2002):

$$m_w = p_w \frac{\partial S_w}{\partial x} - F_{ow} + M_{wm}, \qquad m_o = p_o \frac{\partial S_o}{\partial x} + F_{ow} + M_{om}, \tag{8}$$

where F_{ow} represents the drag force exerted by the water phase on the oil phase. The oil must necessarily exert an equal and opposite force, $-F_{ow}$, on the water phase. The terms M_{om} and M_{wm} denote interaction forces between the fluids and the porous media for oil and water, respectively. The terms $p_w \partial S_w / \partial x$ and $p_o \partial S_o / \partial x$ represent interfacial forces arising from an averaging process. The drag force and the friction forces between fluid and rock are modeled as (Preziosi and Farina, 2002; Ambrosi and Preziosi, 2002):

$$F_{ow} = R(v_w - v_o), \tag{9}$$

$$M_{im} = -R_i v_i, \qquad (i = w, o), \tag{10}$$

Thus, the force exerted between fluid and fluid and between rock and fluid is proportional to the difference in their interstitial velocities. The coefficients R, R_i, all non-negative, will be specified later. Combination of Eqs. (6) through (9), where the chain rule is applied to Eq. (6) and $\tau_i = 0$, results in:

$$S_w \frac{\partial p_w}{\partial x} = -R_w v_w + R(v_o - v_w), \qquad S_o \frac{\partial p_o}{\partial x} = -R_o v_w - R(v_o - v_w), \tag{11}$$

where the right hand side of the equations represent matrix-fluid and fluid-fluid interaction. Solving for the interstitial velocities and inserting these into (4), yields:

$$u_w = -\widehat{\lambda}_{ww} \frac{\partial p_w}{\partial x} - \widehat{\lambda}_{ow} \frac{\partial p_o}{\partial x}, \qquad u_o = -\widehat{\lambda}_{ow} \frac{\partial p_w}{\partial x} - \widehat{\lambda}_{oo} \frac{\partial p_o}{\partial x}, \tag{12}$$

as generalized flux-pressure gradient relations. Note that we have introduced generalized diagonal and cross term mobilities $\widehat{\lambda}_{ww}, \widehat{\lambda}_{oo}$ and $\widehat{\lambda}_{ow}$ defined by:

$$\widehat{\lambda}_{ww} = \frac{S_w^2(R_o + R)}{R_o R_w + R(R_o + R_w)}\varphi_e, \tag{13}$$

$$\widehat{\lambda}_{oo} = \frac{S_o^2(R_w + R)}{R_o R_w + R(R_o + R_w)}\varphi_e, \tag{14}$$

$$\widehat{\lambda}_{ow} = \frac{S_w S_o R}{R_o R_w + R(R_o + R_w)}\varphi_e. \tag{15}$$

Using the capillary pressure relation (5) we can write the phase and total fluxes as:

$$u_w = -\widehat{\lambda}_w \frac{\partial p_w}{\partial x} - \widehat{\lambda}_{ow}\frac{\partial p_c}{\partial x}, \tag{16}$$

$$u_o = -\widehat{\lambda}_o \frac{\partial p_w}{\partial x} - \widehat{\lambda}_{oo}\frac{\partial p_c}{\partial x}, \tag{17}$$

$$u_T = u_w + u_o = -\widehat{\lambda}_T \frac{\partial p_w}{\partial x} - \widehat{\lambda}_o \frac{\partial p_c}{\partial x}, \tag{18}$$

where the following notation is defined for generalized phase mobilities $\widehat{\lambda}_w, \widehat{\lambda}_o$ and total mobility $\widehat{\lambda}_T$:

$$\widehat{\lambda}_w = \widehat{\lambda}_{ww} + \widehat{\lambda}_{wo} = \frac{S_w^2 R_o + S_w R}{R_o R_w + R(R_o + R_w)}\varphi_e, \tag{19}$$

$$\widehat{\lambda}_o = \widehat{\lambda}_{ow} + \widehat{\lambda}_{oo} = \frac{S_o^2 R_w + S_o R}{R_o R_w + R(R_o + R_w)}\varphi_e, \tag{20}$$

$$\widehat{\lambda}_T = \widehat{\lambda}_o + \widehat{\lambda}_w = \frac{S_w^2 R_o + S_o R_w + R}{R_o R_w + R(R_o + R_w)}\varphi_e. \tag{21}$$

From (18), the water pressure gradient can be expressed and used to give updated flux expressions:

$$\frac{\partial p_w}{\partial x} = -\frac{1}{\widehat{\lambda}_T}u_T - \left(1 - \frac{\widehat{\lambda}_w}{\widehat{\lambda}_T}\right)\frac{\partial p_c}{\partial x}, \tag{22}$$

$$u_w = u_T \widehat{f}_w + W\frac{\partial p_c}{\partial x}, \tag{23}$$

$$u_o = u_T \widehat{f}_o - W\frac{\partial p_c}{\partial x}, \tag{24}$$

$\widehat{f}_w$ is the generalized fractional flow function for water and W is a generalized mobility coefficient with definitions:

$$\widehat{f}_w = \frac{\widehat{\lambda}_w}{\widehat{\lambda}_T} = \frac{S_w^2 R_o + S_w R}{S_w^2 R_o + S_o^2 R_w + R}, \tag{25}$$

$$W(S_w) = \widehat{f}_w \widehat{\lambda}_o - \widehat{\lambda}_{ow} = \frac{S_w^2 S_o^2 \varphi_e}{S_w^2 R_o + S_o^2 R_w + R}. \tag{26}$$

If the water flux from Eq. (23) is inserted into the conservation equation for water, (1), we get:

$$\frac{\partial(\varphi s_w)}{\partial t} = -\frac{\partial(u_T \widehat{f}_w)}{\partial x} - \frac{\partial}{\partial x}\left(W\frac{\partial p_c}{\partial x}\right). \tag{27}$$

The oil transport equation can be replaced by the following pressure equation which is found by adding the conservation laws in (1)

$$\frac{\partial u_T}{\partial x} = 0 \tag{28}$$

and using the definition of u_T in (18). equations (25)–(28) constitute the generalized model.

2.1.2. Comparison with conventional approach

The generalized model can be directly compared with a conventional Darcy model which can be written as follows:

$$\frac{\partial(\varphi s_w)}{\partial t} = -\frac{\partial(u_T f_w)}{\partial x} - \frac{\partial}{\partial x}\left(f_w \lambda_o \frac{\partial p_c}{\partial x}\right). \tag{29}$$

Here standard definitions of mobility and fractional flow function would be used:

$$\lambda_i = k_{ri}/\mu_i, \qquad \lambda_T = \lambda_o + \lambda_w, \qquad f_w = \lambda_w/\lambda_T \tag{30}$$

As long as generalized and conventional mobilities are the same ($\widehat{\lambda}_w = \lambda_w$ and $\widehat{\lambda}_o = \lambda_o$), the two approaches would give same behavior except for the key difference seen by the extra term $-\widehat{\lambda}_{ow}$ that is included in W for the generalized model.

2.1.3. Specification of interaction terms

Specification of the interaction terms R and $R_i (i = w, o)$ is needed to obtain explicit analytical expressions for the generalized phase mobilities. The solid-fluid interaction terms should obey $R_i \propto \mu_i \varphi_e / k$ to be consistent with conventional (Darcy) modelling. The following relations were included (Standnes et al., 2017; Standnes and Andersen, 2017; Qiao et al., 2018):

$$R_w = I_w S_w^{\alpha}\frac{\mu_w}{k}\varphi_e, \qquad R_o = I_o S_o^{\beta}\frac{\mu_o}{k}\varphi_e, \qquad R = I S_o S_w \frac{\mu_o \mu_w}{k}\varphi_e. \tag{31}$$

α and β are saturation exponents, I_w and I_o are coefficients that characterize the magnitude of solid-fluid interaction (friction), while I is a coefficient characterizing the magnitude of fluid-fluid coupling (drag) and are assumed independent of saturation and properties of the fluids and rock. The stated parameters have no dimension, except I which has unit $(\text{Pa s})^{-1}$.

2.2. Generalized relative permeabilities

In this section we derive generalized relative permeabilities based on the generalized modelling approach. The relative permeability formulation requires that we consider special flow conditions where the fluxes or pressure gradients of the two phases can be related. The case for co-current flow has been presented previously in Standnes et al. (2017); Qiao et al. (2018), but is briefly derived also here in Sec. 2.2.1. The case for counter-current flow where opposite fluxes are used for defining the flow conditions is derived here for the first time in Sec. 2.2.2. Relations between the co- and counter-current relative permeabilities are derived in Sec. 2.2.3.

2.2.1. Co-current flow

Co-current flow is typical during standard coreflooding experiments. We assume oil and water are co-injected in same direction. There is then a direct link at steady state (when $\partial_t s_i = 0$) between the generalized and conventional model allowing generalized relative permeabilities accounting for viscous coupling to be derived (assuming negligible capillary end effects (Rapoport and Leas, 1953; Andersen et al., 2017b) e.g. by using high injection rate). The pressure gradient will be identical for both phases, yielding the following flux relations from (12):

$$u_w = -\widehat{\lambda}_w \frac{\partial p}{\partial x}, \qquad u_o = -\widehat{\lambda}_o \frac{\partial p}{\partial x}. \tag{32}$$

The generalized mobilities $\widehat{\lambda}_w$ and $\widehat{\lambda}_o$ then represent mobilities that would be measured in a co-current relative permeability measurement. From this we obtain generalized co-current relative permeabilities:

$$\widehat{k}_{rw}^{co} = \frac{\mu_w}{k}\widehat{\lambda}_w = \frac{S_w^{2-\alpha}\left(I_o + I S_o^{1-\beta}\mu_w\right)}{I_o I_w + I\left(I_o S_o S_w^{1-\alpha}\mu_o + I_w S_o^{1-\beta} S_w \mu_w\right)}, \tag{33}$$

$$\widehat{k}_{ro}^{co} = \frac{\mu_o}{k}\widehat{\lambda}_o = \frac{S_o^{2-\beta}\left(I_w + I S_w^{1-\alpha}\mu_o\right)}{I_o I_w + I\left(I_o S_o S_w^{1-\alpha}\mu_o + I_w S_o^{1-\beta} S_w \mu_w\right)}. \tag{34}$$

It is evident that the generalized relative permeabilities are not only

functions of saturations, but also depend on fluid viscosities when $I > 0$. Viscosity dependence has been suggested previously by several authors (Yuster, 1951; Odeh, 1959; Lefebvre du Prey, 1973; Nejad et al., 2011). The resulting relative permeability endpoints are

$$\widehat{k}_{rw}^{co}(S_w = 0) = 0, \qquad \widehat{k}_{rw}^{co}(S_w = 1) = \frac{1}{I_w}, \tag{35}$$

$$\widehat{k}_{ro}^{co}(S_w = 0) = \frac{1}{I_o}, \qquad \widehat{k}_{ro}^{co}(S_w = 1) = 0. \tag{36}$$

As a special case, we note that if the fluid-fluid interaction coefficient I is set to 0, the co-current relative permeability expressions simplify to Corey-type Corey et al. (1954); Brooks and Corey (1964) expressions:

$$\widehat{k}_{rw}^{co} = \frac{S_w^{2-\alpha}}{I_w}, \qquad \widehat{k}_{ro}^{co} = \frac{S_o^{2-\beta}}{I_o}. \tag{37}$$

where the end points are as stated above, and the Corey exponents n_o, n_w are related to α, β by:

$$n_w = 2 - \alpha, \qquad n_o = 2 - \beta. \tag{38}$$

Assuming Corey exponents typically in the range of 1.5–5, typical values of α, β would then be 0.5 to −3.

2.2.2. Counter-current flow

When the flow mode is changed to purely counter-current with no net flux in any direction ($u_T = 0$), then due to conservation of volume, we have fluxes of equal magnitude, but with opposite directions:

$$u_w = -u_o. \tag{39}$$

That is the typical case in all-faces-open or one-face-open SI experiments Mason and Morrow (2013). The fluxes can be expressed using (12):

$$-\widehat{\lambda}_{ww}\frac{\partial p_w}{\partial x} - \widehat{\lambda}_{ow}\frac{\partial p_o}{\partial x} = \widehat{\lambda}_{ow}\frac{\partial p_w}{\partial x} + \widehat{\lambda}_{oo}\frac{\partial p_o}{\partial x}. \tag{40}$$

The pressure gradients are then separated and expressed relative to each other:

$$\frac{\partial p_o}{\partial x} = -\frac{\widehat{\lambda}_w}{\widehat{\lambda}_o}\frac{\partial p_w}{\partial x}, \qquad \frac{\partial p_w}{\partial x} = -\frac{\widehat{\lambda}_o}{\widehat{\lambda}_w}\frac{\partial p_o}{\partial x}. \tag{41}$$

The pressure gradient expressions above can now be inserted back into the flux relations (12) and provide a relation for how a phase's flux is proportional to its own pressure gradient under these flow conditions:

$$u_w = -\widehat{\lambda}_w\left[\frac{\widehat{\lambda}_{ww}}{\widehat{\lambda}_w} - \frac{\widehat{\lambda}_{ow}}{\widehat{\lambda}_o}\right]\frac{\partial p_w}{\partial x}, \qquad u_o = -\widehat{\lambda}_o\left[\frac{\widehat{\lambda}_{oo}}{\widehat{\lambda}_o} - \frac{\widehat{\lambda}_{ow}}{\widehat{\lambda}_w}\right]\frac{\partial p_o}{\partial x}. \tag{42}$$

If we now compare equations (42) and (42) to the co-current versions (32) and (32), we see that they differ by the factor enclosed in square brackets. Further, we again note that the proportionality factor between u_i and $\partial p_i/\partial x$ should be $-kk_{ri}/\mu_i$, where $(i = w, o)$. This is used to obtain the following generalized relative permeabilities for purely counter-current flow:

$$\widehat{k}_{rw}^{cou} = \frac{\mu_w}{k}\widehat{\lambda}_w\left[\frac{\widehat{\lambda}_{ww}}{\widehat{\lambda}_w} - \frac{\widehat{\lambda}_{ow}}{\widehat{\lambda}_o}\right] = \widehat{k}_{rw}^{co}C_w, \quad C_w = \left[\frac{\widehat{\lambda}_{ww}}{\widehat{\lambda}_w} - \frac{\widehat{\lambda}_{ow}}{\widehat{\lambda}_o}\right], \tag{43}$$

$$\widehat{k}_{ro}^{cou} = \frac{\mu_o}{k}\widehat{\lambda}_o\left[\frac{\widehat{\lambda}_{oo}}{\widehat{\lambda}_o} - \frac{\widehat{\lambda}_{ow}}{\widehat{\lambda}_w}\right] = \widehat{k}_{ro}^{co}C_o, \quad C_o = \left[\frac{\widehat{\lambda}_{oo}}{\widehat{\lambda}_o} - \frac{\widehat{\lambda}_{ow}}{\widehat{\lambda}_w}\right]. \tag{44}$$

As seen, the counter-current relative permeabilities $\widehat{k}_{ri}^{cou}$ are expressed using the co-current relative permeabilities $\widehat{k}_{ri}^{co}$ from eqs. (33) and (34), multiplied by the factors in square brackets which will be denoted C_o, C_w. It is equivalent whether we study the properties of $\widehat{k}_{ri}^{cou}$ or C_i and we hence choose to focus on C_i for now.

2.2.3. Relations between co- and counter-current generalized relative permeabilities

The first interesting observation made is that by collecting the terms in (43) to one fraction and using the diagonal and cross term mobilities we obtain that C_w and C_o give identical expressions:

$$C_w = \frac{\widehat{\lambda}_{ww}}{\widehat{\lambda}_w} - \frac{\widehat{\lambda}_{ow}}{\widehat{\lambda}_o} = \frac{\widehat{\lambda}_{oo}\widehat{\lambda}_{ww} - \widehat{\lambda}_{ow}\widehat{\lambda}_{ow}}{(\widehat{\lambda}_{ww} + \widehat{\lambda}_{ow})(\widehat{\lambda}_{oo} + \widehat{\lambda}_{ow})} \tag{45}$$

$$C_o = \frac{\widehat{\lambda}_{oo}}{\widehat{\lambda}_o} - \frac{\widehat{\lambda}_{ow}}{\widehat{\lambda}_w} = \frac{\widehat{\lambda}_{oo}\widehat{\lambda}_{ww} - \widehat{\lambda}_{ow}\widehat{\lambda}_{ow}}{(\widehat{\lambda}_{ww} + \widehat{\lambda}_{ow})(\widehat{\lambda}_{oo} + \widehat{\lambda}_{ow})} \tag{46}$$

In other words, the co-current and counter-current relative permeabilities are modified by the same factor for a given oil-water saturation configuration whether we consider the oil or water phase. Note that this holds true for any generalized formulation with equal cross term mobilities.

Note also that if $\widehat{\lambda}_{ow} = 0$ the expressions simplify to $C_i = 1$, i.e. the co-current and counter-current relative permeabilities are identical.

If the terms $\widehat{\lambda}_{oo}, \widehat{\lambda}_{ww}, \widehat{\lambda}_{ow}$ were assigned arbitrary values, it would appear that C_i can be negative, which would mean that also the relative permeabilities would be negative. It is also not clear what upper limit C_i can take. However, by using the definitions in (13) we obtain:

$$C_i = \frac{S_o S_w(R_w R_o + R(R_w + R_o))}{(S_w R_o + R)(S_o R_w + R)} \tag{47}$$

$$= \frac{S_o S_w R_o R_w + S_o S_w R_w R + S_o S_w R_o R}{S_o S_w R_o R_w + S_o R_w R + S_w R_o R + R^2} \tag{48}$$

As seen, all terms are positive, indicating that positive counter-current relative permeabilities are always obtained. Further, comparing term by term in the expanded expression, the denominator is always less than the nominator if $R \neq 0$ (equal otherwise) demonstrating that $C_i \leq 1$ and that the counter-current relative permeabilities must be lower or equal to the co-current relative permeabilities.

$$C_i = \frac{I_w I_o + I\left(I_w S_o^{1-\beta} S_w \mu_w + I_o S_o S_w^{1-\alpha}\mu_o\right)}{\left(I_o + I S_o^{1-\beta}\mu_w\right)\left(I_w + I S_w^{1-\alpha}\mu_o\right)} \tag{49}$$

As expected, when setting $I = 0$ (which results in $\widehat{\lambda}_{ow} = 0$) we obtain:

$$C_i(S_o, S_w; I = 0) = 1, \tag{50}$$

Further, at the end points, C_i consequently gives a non-unity reduction factor for any $I \neq 0$:

$$C_i(S_w = 0) = \frac{I_o}{I_o + I\mu_w}, \qquad C_i(S_w = 1) = \frac{I_w}{I_w + I\mu_o}, \tag{51}$$

which from (35) and (36) gives the following counter-current relative permeability end points:

$$\widehat{k}_{rw}^{cou}(S_w = 0) = 0, \qquad \widehat{k}_{rw}^{cou}(S_w = 1) = \frac{1}{I_w + I\mu_o}, \tag{52}$$

$$\widehat{k}_{ro}^{cou}(S_w = 0) = \frac{1}{I_o + I\mu_w}, \qquad \widehat{k}_{ro}^{cou}(S_w = 1) = 0. \tag{53}$$

2.3. Capillary pressure correlation

The capillary pressure function will be assumed to follow Leverett J-function scaling (Bear, 2013; Leverett, 1941):

$$p_c = \sigma_{ow}\sqrt{\frac{\varphi}{k}}J(S_w), \tag{54}$$

where σ_{ow} is oil-water interfacial tension and $J(S_w)$ is a dimensionless saturation function. The following expression by Andersen et al. (2017a) is used for $J(S_w)$:

$$J(S_w) = \frac{a_1}{1 + k_1 S_w} - \frac{a_2}{1 + k_2(1 - S_w)} + c, \tag{55}$$

where $a_1, a_2, k_1, k_2 > 0$ and c are curve-fitting parameters.

3. Analytical solutions

3.1. Solution for 1-D, co-current flow

The analytical solution for two-phase, 1-D, co-current displacement was first presented by Buckley and Leverett (1942). It relies on a mass balance equation with a saturation dependent advective term only (no capillary forces) and the method of characteristics (briefly outlined in the following). From the full set of equations we ignore the capillary diffusion term in (27) and assume a predefined injected flux u_T (we then do not need to solve the pressure equation (28)) and obtain:

$$\varphi \frac{\partial s_w}{\partial t} = - u_T \frac{\partial \widehat{f_w}}{\partial x} \tag{56}$$

$$S_w(x, t = 0) = 0, \qquad S_w(x = 0, t) = 1, \tag{57}$$

Water injection is assumed together with initial connate water saturation. This corresponds to a Buckley-Leverett system as defined above.

Since $S_w = S_w(x, t)$ the path of a fixed saturation can be expressed as:

$$dS_w = \frac{\partial S_w}{\partial x} dx + \frac{\partial S_w}{\partial t} dt = 0. \tag{58}$$

and substituting this into (56) yields:

$$\left(\frac{dx}{dt}\right)_{S_w} = \frac{u_T}{\varphi} \left(\frac{d\widehat{f_w}}{dS_w}\right)_{S_w}, \qquad x_{S_w} = \frac{u_T t}{\varphi} \left(\frac{d\widehat{f_w}}{dS_w}\right)_{S_w}, \qquad (S_w \geq S_f), \tag{59}$$

where the latter equation follows from integrating the former.

As noted, this solution is only valid for saturations above a possible shock front saturation S_f. Direct application of the frontal advance equation (59) over the entire saturation range may produce an unphysical solution. In most cases in the literature the fractional flow function has a peak in f' while $f' = 0$ at $S_w = 0$ and $S_w = 1$. In other words, intermediate saturations catch up with low saturations and a shock front is formed. The speed and saturation range of the front is typically given by mass conservation and flux continuity (continuity with the physical solution). If the conditions are as described with a unique peak in f', then S_f can be found at the tangent point on f_w drawn from $S_w = 0$ which is equivalent to solving the following equation for S_f, Buckley and Leverett (1942):

$$\frac{d\widehat{f_w}}{dS_w}\Big|_{S_f} = \frac{\widehat{f_w}(S_f)}{S_f}. \tag{60}$$

Hence, the position of the shock (and all saturation in its range) is

$$x_{S_w} = \frac{u_T t}{\varphi} \left(\frac{d\widehat{f_w}}{dS_w}\right)\Big|_{S_f}, \qquad (0 < S_w < S_f). \tag{61}$$

Although both standard and generalized problems can give exceptions to this rule (e.g. several fronts), we will for simplicity only consider cases where it is applicable.

3.2. Solution for counter-current spontaneous imbibition

In the case of counter-current spontaneous imbibition, a no-flow boundary and (necessarily) zero advective forces implies that the pressure equation is replaced by the constraint $u_T = 0$ and thus $u_w = -u_o$. The system of consideration is then:

$$\varphi \frac{\partial s_w}{\partial t} = \frac{\partial}{\partial x}\left[D(s_w) \frac{\partial s_w}{\partial x}\right], \tag{62}$$

where a capillary diffusion coefficient $D(s_w)$ has been defined:

$$D(s_w) = - W \frac{dp_c}{ds_w}. \tag{63}$$

Note that the introduction of counter-current relative permeabilities also allows to use the conventional definition:

$$D(s_w) = - \widehat{\lambda_o} \widehat{f_w} \frac{dp_c}{ds_w} = - k \frac{\widehat{\frac{k_{ro}}{\mu_o}} \widehat{\frac{k_{rw}}{\mu_w}}}{\widehat{\frac{k_{ro}}{\mu_o}} + \widehat{\frac{k_{rw}}{\mu_w}}} \frac{dp_c}{ds_w}. \tag{64}$$

The relevant initial and boundary conditions for a finite system are:

$$s_w(x, t = 0) = s_{wc}, \tag{65}$$

$$s_w(x = 0, t) = s_{eq}, \tag{66}$$

$$\partial_x s_w|_{x=L} = 0, \tag{67}$$

where s_{eq} is a fixed saturation at the boundary corresponding to zero capillary pressure. In our case $s_{eq} = 1 - s_{or}$, since for a strongly water-wet material, a positive capillary pressure exists for the whole mobile saturation range. Derivations of analytical solutions to (62) in integral form were found in McWhorter and Sunada (1990) and Schmid and Geiger (2012), however, their analytical solution was based on a semi-infinite porous medium, thus replacing the boundary condition at $x = L$ in (67) with:

$$s_w(x = \infty, t) = s_{wc}. \tag{68}$$

Hence, the analytical solution will only be valid for the finite system until the imbibition front reaches the closed end boundary. McWhorter and Sunada (1990) made no limiting assumptions regarding the functional forms contained in $D(s_w)$, but specified a boundary condition for the inflow at the open end as:

$$u_{w0} = u_w(x = 0, t) = A t^{-1/2}, \tag{69}$$

where A is referred to as the inflow parameter, and for a given system is a constant that describes the system's ability to imbibe water. A can be found from:

$$A^2 = \frac{\varphi}{2} \int_{s_{wc}}^{s_{eq}} \frac{(s_w - s_{wc}) D(s_w)}{F(s_w)} ds_w, \tag{70}$$

and is related to the cumulative water imbibed, Q_w, by

$$Q_w(t) = \int_0^t u_{w0}(t) dt = 2 A t^{1/2}. \tag{71}$$

$F(s_w)$ represents a fractional flow function for counter-current spontaneous imbibition and can be regarded as the capillary counterpart to $f_w(s_w)$ (Schmid and Geiger, 2012). It is defined as:

$$F(x, t) = \frac{u_w(x, t)}{u_{w0}(t)}, \tag{72}$$

meaning it describes the ratio of water flux at some position x to the water flux at the inlet, u_{w0} (i.e. the maximum water flux) at similar times t. $F(s_w)$ is obtained by solving the implicit integral equation:

$$F(s_w) = 1 - \left[\int_{s_w}^{s_{eq}} \frac{(\beta - s_w) D(\beta)}{F(\beta)} d\beta\right] \cdot \left[\int_{s_{wc}}^{s_{eq}} \frac{(s_w - s_{wc}) D(s_w)}{F(s_w)} ds_w\right]^{-1}, \tag{73}$$

where the integration variable β represents water saturations. When $F(s_w)$ is known, its derivative can be found from numerical differentiation and A can be found from (70). The solution to (62) with the

specified boundary conditions (65), (66) and (68) can then be written in terms of the inflow parameter, A, and the derivative of $F(s_w)$:

$$x(s_w,t)=\frac{2A}{\varphi}F'(s_w)t^{1/2}=\frac{Q_w(t)}{\varphi}F'(s_w). \tag{74}$$

This is used to construct saturation profiles and to calculate oil recovery, since the volume of produced oil must be equal to the total amount of imbibed water in the purely counter-current process considered here.

As mentioned, the analytical solution is only valid as long as the saturation front has not reached the closed end boundary $x = L$. The time when the front reaches the end of the core is denoted t^* and is obtained by setting $x(s_w,t)=L$ in Eq. (74), (March et al., 2016):

$$t^*=\left(\frac{L\varphi}{2AF'(s_{wr})}\right)^2. \tag{75}$$

Since $F(s_w)$ given by Eq. (73) depends on itself, it has to be computed using an iterative procedure (McWhorter and Sunada, 1990; Nooruddin and Blunt, 2016). The first step is to calculate the capillary diffusion coefficient, $D(s_w)$ from known relative permeabilities and capillary pressure curves using (70). The iterative computations are then initiated by assuming starting guesses $F(s_w)=1$ for all values of s_w. Using this first guess, the integral in (73) can be computed, and an updated $F(s_w)$ is found. The updated $F(s_w)$ can be inserted into the integral in (73) to compute the next iteration. The iterative process continues until the difference between the updated and previous values satisfies a specified tolerance condition for convergence.

4. Results

4.1. Base case input parameters

Numerical solutions for the transient generalized model (27) and (28) were validated in Qiao et al. (2018) numerically by comparing against solutions from commercial software for co-current flow where co-current relative permeabilities could be assumed. The model was parameterized in Andersen et al. (2019a); Qiao et al. (2018) by matching the experimental results of Bourbiaux and Kalaydjian (1990) where viscous coupling could be quantified based on co- and counter-current flow under otherwise identical conditions. Particularly, accurately measured co-current relative permeabilities, the imbibition capillary pressure function and a counter-current SI experiment were used to systematically and uniquely determine the parameters involved in the generalized model. The same input parameters are applied here and listed in Table 1. The only exception is the parameters used to generate the capillary pressure curve, where the J-function was stopped at the threshold pressure (and the decline to zero at $S = 1$ was ignored) to make a smoother function. The J-function and co-current relative permeabilities resulting of these parameters are plotted in Fig. 1. Unless otherwise is indicated, the input parameters in Table 1 are assumed.

Table 1
Base case input parameters.

L	0.29 m	I_w	23.3
φ	0.233	I_o	2.15
s_{wr}	0.4	I	2500 $(\text{Pa}\cdot\text{s})^{-1}$
s_{or}	0.425	α	−0.0
μ_w	1.2 mPa·s	β	1.0
μ_o	1.5 mPa·s	a_1	0.56
k	118 mD	a_2	0.66
σ	15.8 mN/m	k_1	1.25
		k_2	0.08
		c	0.55

4.2. Forced imbibition

In this section, the effect of viscous coupling on forced imbibition is studied. Since this is a purely co-current flow setting, only the generalized co-current relative permeabilities are used.

Conventional relative permeabilities will in the following be defined such that a specified value of I and the base case viscosities characterizes the viscous coupling of the fluid-rock system when the relative permeabilities were measured. A different I is assumed to give different measured curves. The conventional assumption is that the measured relative permeabilities will not change with flow regime or viscosities. The *generalized* relative permeabilities account for that changing the viscosities or flow regime will change the extent of viscous coupling (for the given I) and hence change the relative permeabilities.

In Fig. 2 we present relative permeabilities and corresponding fractional flow functions for different combinations of fluid viscosities (where the oil viscosity μ_o is varied by a factor 1, 10 or 100 from its reference value) and fluid-fluid interaction coefficients I equal to 250, 2500 and 25000 (Pa s)-1. For a given value of I (a given column) it is assumed co-current relative permeabilities have been measured at the reference oil viscosity and are given by (33) and (34). Using a conventional approach (*con*) the curves are held fixed and any modifications to the conventional fractional flow function (dashed lines) are due to changes in viscosity ratio only.

When the reference oil viscosity is used, the generalized model and conventional model yield identical relative permeability functions (red). The conventional relative permeabilities are not explicitly plotted since they are identical to the generalized relative permeabilities at the base viscosity. Varying viscosity will affect the generalized relative permeabilities and thus introduce an additional impact on the generalized fractional flow function (full lines).

At a low value of $I = 250$ (Pa s)-1 (10 times lower than the base value) there is little fluid-fluid interaction and hence little sensitivity to viscosity on the generalized relative permeability functions which remain closely gathered. We note that for low I the generalized relative permeability functions approach Corey functions, according to (37). However, as seen in both (33), (34) and Fig. 2 the increased fluid viscosities can increase the importance of viscous coupling. At higher values of I the impact of fluid viscosities on relative permeabilities is more pronounced. When the oil becomes more viscous it will tend to travel slow compared to the water. In accordance with momentum transfer we note that water then will be decelerated by the oil, while oil gets accelerated by the water and in effect oil relative permeability increases while water relative permeability decreases with increasing oil viscosity. The effect is greater when I is greater.

For $I = 250$ the fractional flow functions are thus also quite similar between the conventional and generalized models, but are lifted for a given saturation as oil viscosity is increased. At strong viscous coupling (high I and viscosity μ_o) any difference in fluid velocities is suppressed and the fractional flow function approaches a straight line indicating that the oil and water travel as a single mixture with same velocity.

The resulting impact on saturation distributions after 0.5 PV injected and recovery vs PV injected is shown in Fig. 3. In accordance with traditional theory, for fixed relative permeability functions (conventional model) higher oil viscosity lowers the front saturation and the saturations behind it, gives earlier water breakthrough and lower recovery with PVs injected. However, the impact of viscosity is less significant when accounting for viscous coupling. In all cases (except the base where there is no difference) the viscous coupling slows down the faster moving fluid and accelerates the slow one and gives an overall more favorable oil displacement compared to the conventional model. For very strong viscous coupling piston-like displacement is obtained with all mobile oil recovered before water breakthrough.

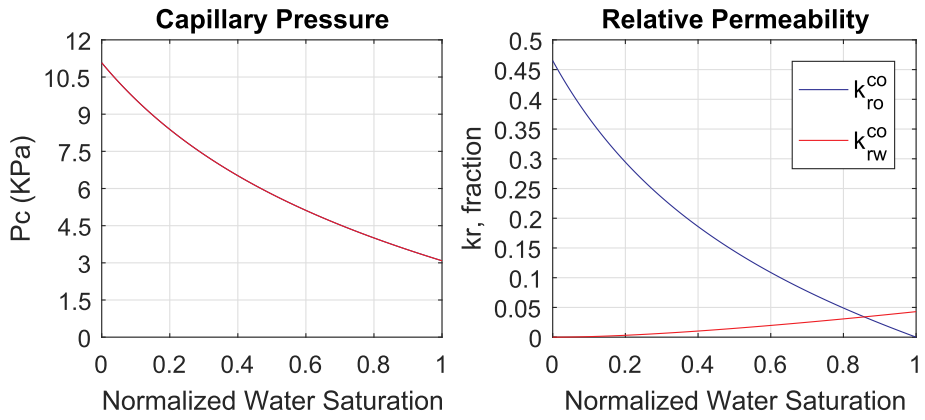

Fig. 1. Capillary pressure (left) and co-currently measured relative permeabilities (right) based on experimental data from Bourbiaux and Kalaydjian (1990).

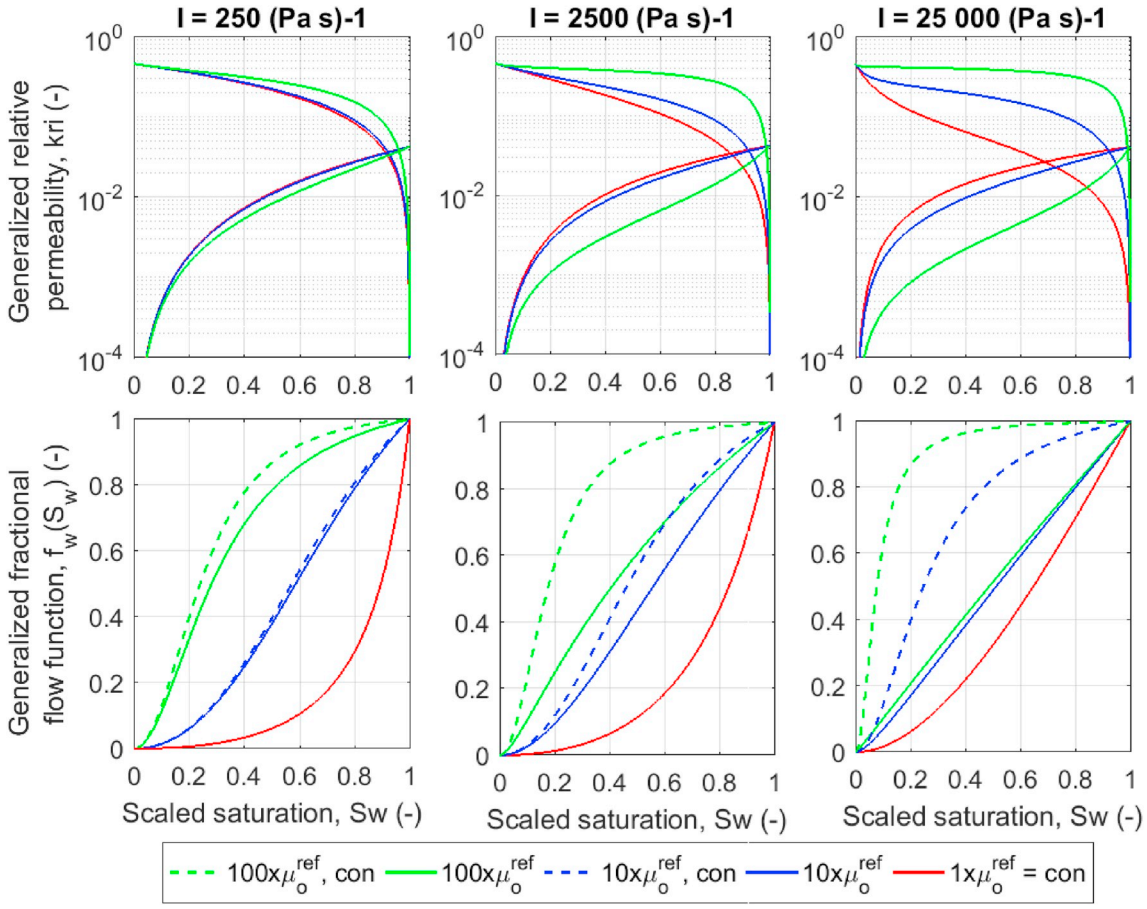

Fig. 2. Top: Co-current relative permeabilities for different oil viscosities and values of I. For all viscosities, the conventional relative permeabilities correspond to the red (generalized) curve (which is not affected by viscosity) obtained at the reference parameters. When viscosities change, the generalized relative permeabilities differ from the conventional. Bottom: Corresponding conventional and generalized fractional flow functions. (For interpretation of the references to colour in this figure legend, the reader is referred to the Web version of this article.)

4.3. Counter-current spontaneous imbibition

When the flow regime is altered from co-to counter-current the relative permeabilities are affected as can be seen by comparing them in Fig. 4 for various combinations of fluid-fluid interaction coefficient I and oil viscosities μ_o. For low values of I (when viscous coupling is less important) there is little difference between the co- and counter-current relative permeabilities, but the difference increases with I and μ_o. Especially, increases in both these parameters reduces the counter-current relative permeability across the entire saturation range compared to the co-current relative permeabilities. The magnitude of the reduction is quantified by the coefficient C_i in (49). Considering (35) with (36) and (52) with (53) it follows that increasing the two parameters directly lower the counter-current relative permeability end points, while the co-current relative permeability end points are not changed. That is also reflected in the figure.

C_i corresponding to the abovementioned cases is plotted in Fig. 5 showing how much the relative permeabilities are reduced by changing

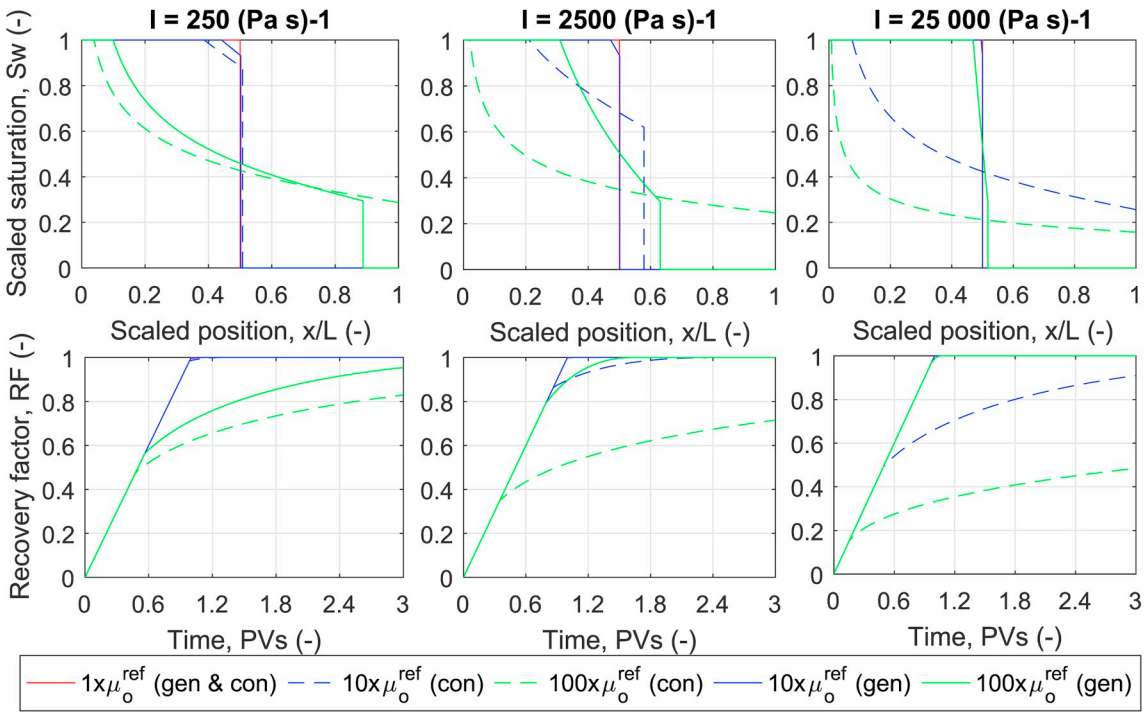

Fig. 3. Top: Saturation distributions after 0.5 PVs were injected assuming different oil viscosities and values of I. The generalized (gen) model is compared to the conventional (con). Bottom: Corresponding recovery vs PVs injected.

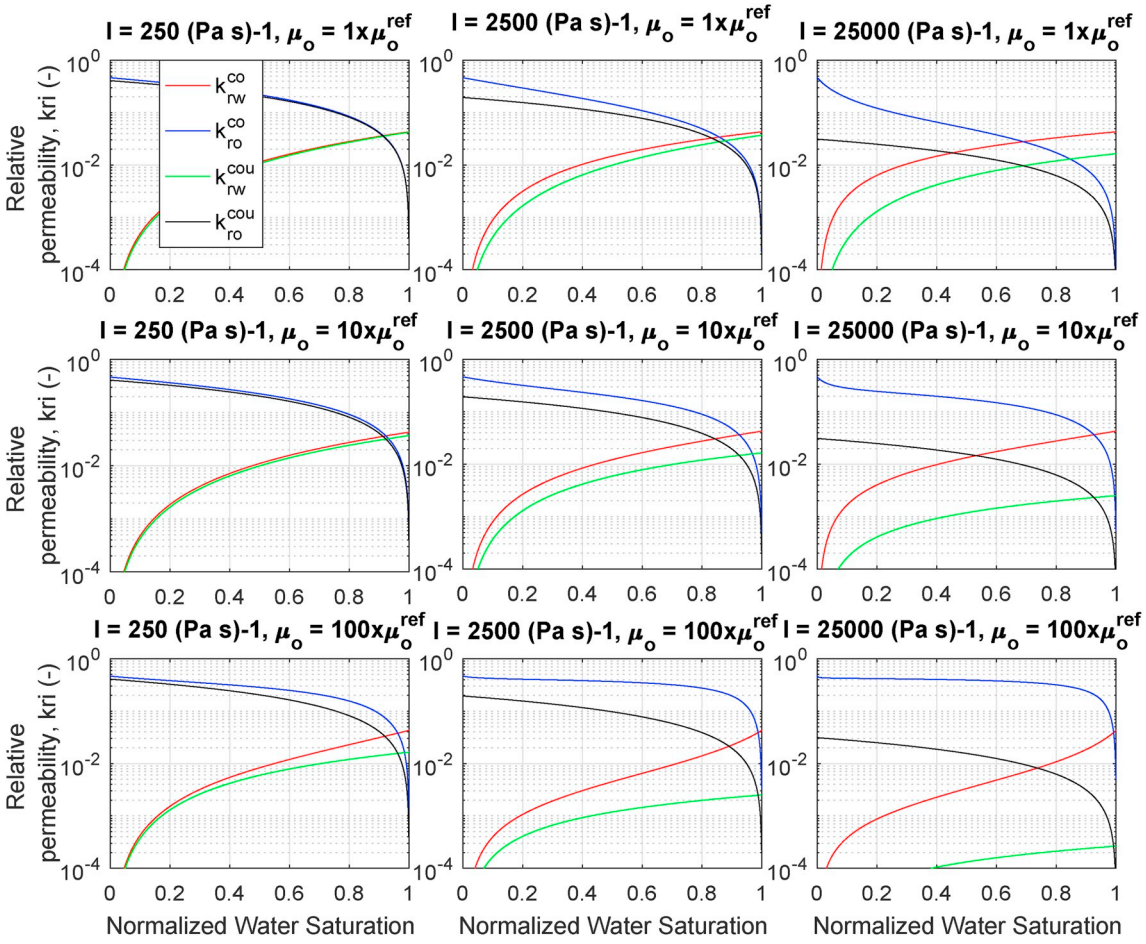

Fig. 4. Comparison of co- and counter-current relative permeabilities for different combinations of I and μ_o.

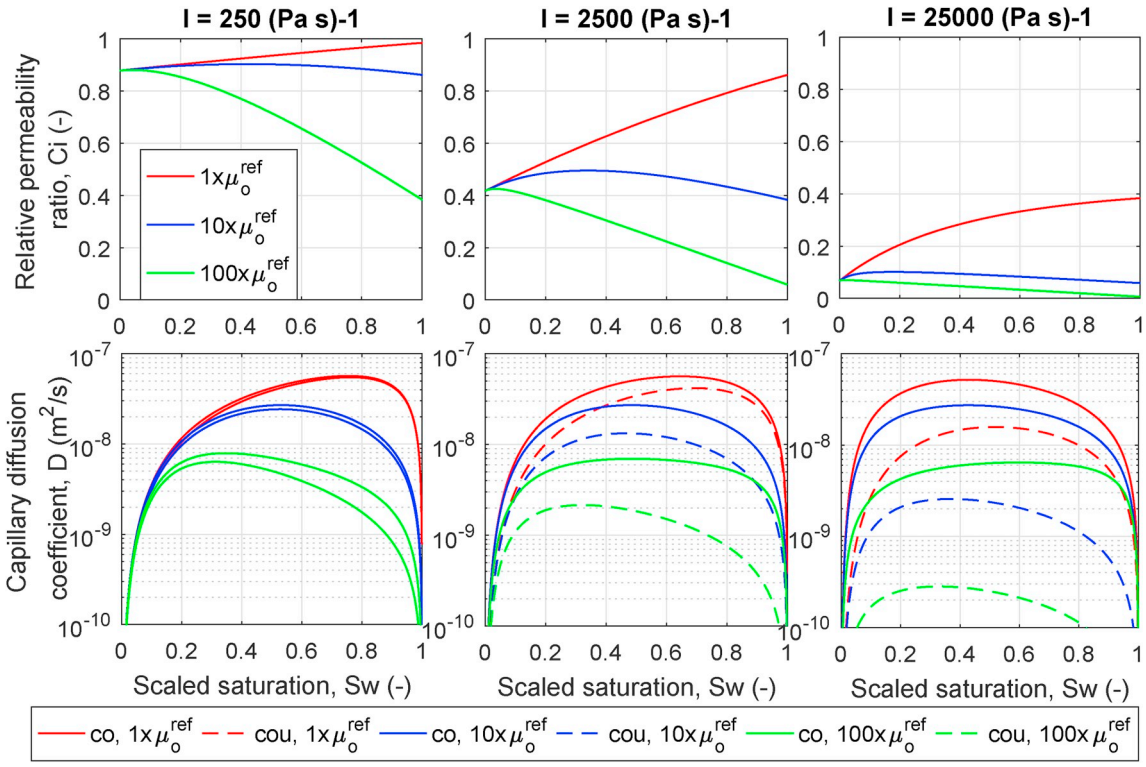

Fig. 5. Top: Coefficient comparing counter-current and co-current relative permeabilities. Bottom: Capillary diffusion coefficient based on co- and counter-current relative permeabilities. The cases are based on the relative permeabilities in Fig. 4.

flow regime. We note that the base case ($I = 2500$ (Pa s)-1 and $\mu_o = \mu_o^{ref}$) corresponds to matching experimental data performed by Bourbiaux and Kalaydjian (1990), as conducted in Andersen et al. (2019a). With our model, both phase relative permeabilities are reduced by a coefficient ranging from 0.4 to 0.85 when the flow regime is switched from co-current to counter-current. In comparison Bourbiaux and Kalaydjian (1990) reduced both curves by a constant factor of 0.7, but did not provide any justification for reducing them by the same factor for both phases and across the entire saturation range. The impact of I and μ_o is also seen on the capillary diffusion coefficient D, in Fig. 5, which is significantly lowered using counter-current relative permeabilities compared to using the co-current relative permeabilities directly.

Based on the presented cases in the above figures we now explore the behavior of the following transient models:

- The generalized model with no-flow boundary which is solved numerically and accounts for viscous coupling.
- The conventional model with no-flow boundary which assumes co-current relative permeabilities and is solved numerically. It does not account for viscous coupling.

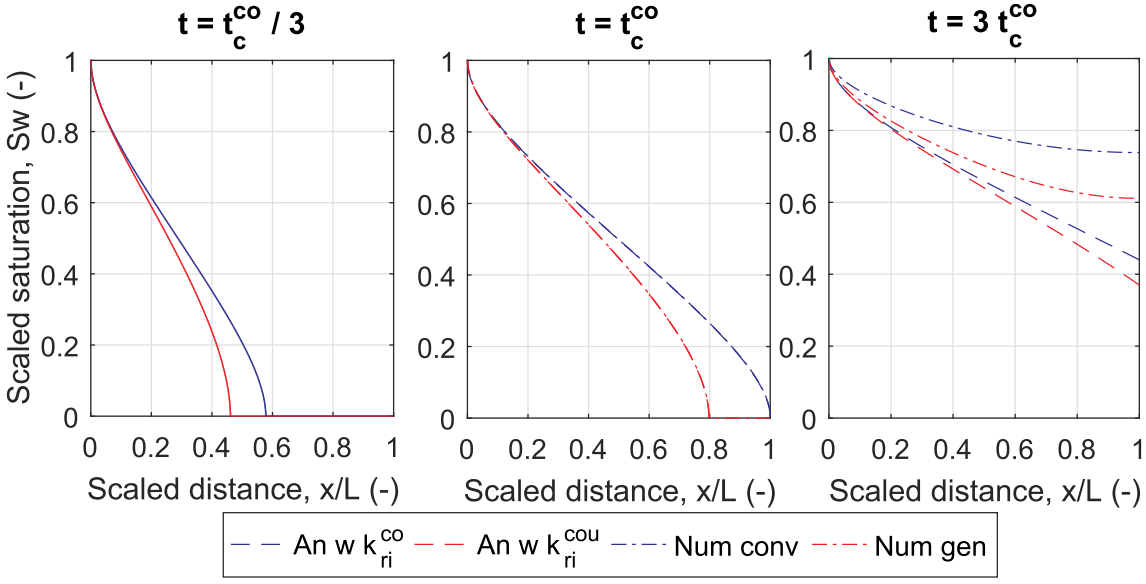

Fig. 6. Saturation distributions for the base case presented at $t = 1/3t_c^{co}, t_c^{co}, 3t_c^{co}$ where t_c^{co} is the time when the front of the model with co-current relative permeabilities reaches the no-flow boundary. Analytical solutions based on a semi-infinite axis are compared with numerical solutions with closed inner boundary.

- The analytical model using counter-current relative permeabilities and thus accounts for viscous coupling, but does not account for the no-flow boundary.
- The analytical model using co-current relative permeabilities and does not account for viscous coupling or the no-flow boundary.

Saturation distributions are shown in Fig. 6 at times $t = 0.33t_c^{co}, t_c^{co}, 3t_c^{co}$, where t_c^{co} is the time when the conventional model water front reaches the no-flow boundary. Some key observations are made:

- For times before the no-flow boundary is met, the two analytical solutions (using flow regime dependent relative permeabilities) coincide perfectly with the two numerical solutions (the generalized model with generalized cross and diagonal mobilities and the conventional model with generalized co-current relative permeabilities).
- The viscous coupling causes a delay in imbibition compared to what would be predicted by directly applying the co-current relative permeabilities in a standard (conventional) model.
- After the no-flow boundary is met, the solutions differ significantly and the analytical solution is not valid.

The impact of the parameters I and μ_o is illustrated on the saturation distributions at $t = t_c^{co}$ using the analytical solutions, see Fig. 7. Note that t_c^{co} can vary from case to case, but before the infinite-acting period is over, the saturation profile is invariant for given input parameters. For low I the solutions applying co- and counter-current relative permeabilities are very similar, but change with viscosity. Especially, higher oil viscosity appears to lower the saturation profile. At higher interaction coefficients the solutions based on counter-current relative permeabilities are more significantly delayed and their front is further away from the no-flow boundary.

The corresponding recovery profiles are shown in Fig. 8. For the base case the analytical solutions with co- or counter-current relative permeabilities are compared with the conventional and generalized numerical solutions, respectively and yield identical results until late times when no-flow boundary conditions become significant. At late times the analytical solutions optimistically predict the square root of time recovery behavior to continue, while the imbibition rate for the numerical solutions declines more rapidly. It is seen that the fluid-fluid interaction causes the SI process to occur more slowly than predicted by using co-current relative permeabilities, in line with the previously shown results.

4.4. Universal scaling

Schmid and Geiger (2012) showed that for given relative permeability and capillary pressure functions, the integral solution to counter-current SI by McWhorter and Sunada (1990) could be scaled using the imbibed volume $Q_w = 2At^{1/2}$ relative to the pore volume φL as follows:

$$t_d = \left(\frac{Q_w}{\varphi L}\right)^2 = \left(\frac{2A}{\varphi L}\right)^2 t = t \Big/ \tau, \qquad \tau = \left(\frac{\varphi L}{2A}\right)^2. \tag{76}$$

This equation shows that the fractional recovery of mobile oil should be equal vs scaled time as long as square root of time behavior is valid (before the no-flow boundaries are encountered).

To demonstrate whether this scaling procedure can account for viscous coupling as done by implementing our counter-current relative permeabilities we here run three different cases termed A, B and C, where for each case the fluid-fluid interaction coefficient I is varied from 0 (no viscous coupling) to 10000 (Pa s)-1 (strong viscous coupling). The relevant input parameters are listed in Table 2 together with the calculated value of τ from (76), while those parameters not specified are given by the reference values in Table 1. The generalized model was solved numerically (thus accounting for both viscous coupling and no-flow boundaries); 200 grid cells were applied. The recovery factor of mobile oil is plotted against absolute time t in Fig. 9 (left) for the different cases. It is seen that the time to reach a given intermediate recovery value spans by roughly one order of magnitude. Especially, for a given case the influence of viscous coupling gives a significant variation in time scales, by up to a factor of 4. The same results are plotted against scaled time $t_d = t/\tau$ in Fig. 9 (right). It is seen that the results overlap completely until late times where boundary effects affect the validity of the scaling assumptions. For precision; the analytical solutions are able to scale (gather) curves:

- that are not affected by viscous coupling but have different curve parameters: cases A, B, C with $I = 0$
- that have various degrees of viscous coupling introduced to the same curve set: e.g. case A with different values of I.
- both with different curve parameters and degree of fluid-fluid interaction (all curves unify).

It can be noted that the time scales τ greatly exceed the time scale when the validity of the scaling terminates. Consistently with Schmid and Geiger (2012) this seems to occur around 0.01 τ with some variation (the simulation results were hence plotted until 0.1 τ). The scaling based

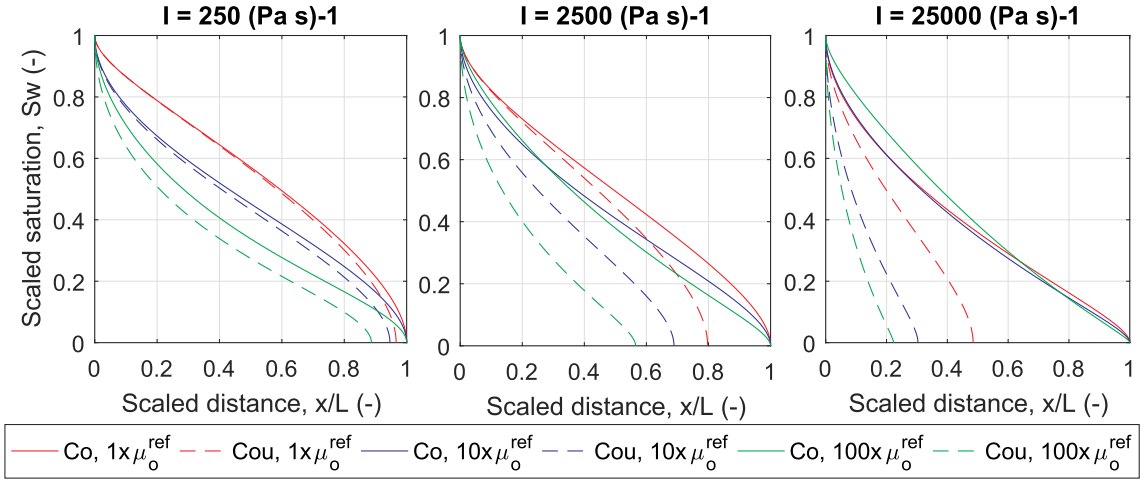

Fig. 7. Saturation distributions calculated for different I and μ_o with the analytical solution for co- and counter-current relative permeabilities evaluated at $t = t_c^{co}$ where t_c^{co} is the time when the front of the model with co-current relative permeabilities reaches the no-flow boundary.

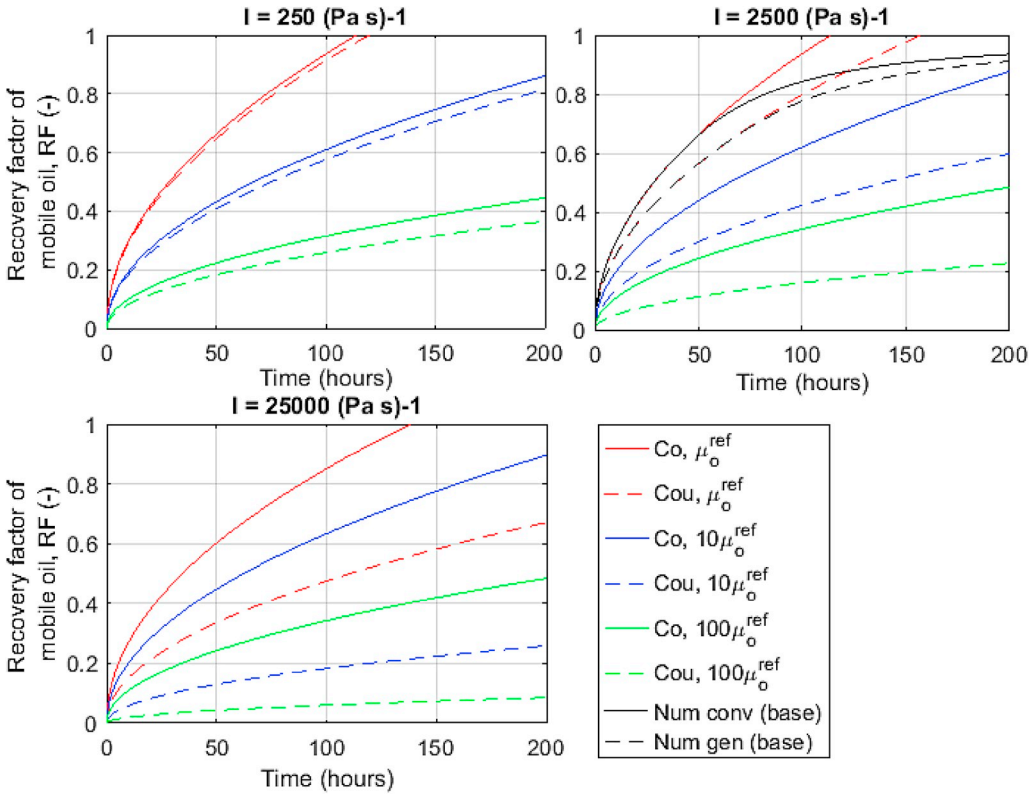

Fig. 8. Recovery factor calculated for different I and μ_o with the analytical solution for co- and counter-current relative permeabilities from 0 to 200 h. Note that the solutions are extrapolated beyond t_c such that the late time behavior is not properly reflecting a closed system. The base case is compared to numerical solutions.

Table 2
Input parameters used for scaling example.

Case	α	β	I_w	I_o	I	τ
	(−)	(−)	(−)	(−)	((Pa s)-1)	(hrs)
A	0.5	−1	20	1	0, 5000, 25000	5130, 7090, 14500
B	−1	0	10	15	0, 5000, 25000	14100, 16200, 24300
C	0	−2	2	2	0, 5000, 25000	3690, 6370, 15600

on the analytical solution can be used to effectively estimate the magnitude of viscous coupling if SI tests are performed using different viscosity combinations on porous media where relative permeability and capillary pressure is measured under reference conditions. Examples of such a work using an explicit time scale is demonstrated in Standnes and Andersen (2017) where viscous coupling was used to explain non-standard experimental trends.

Although the presented analytical solution is valid only until the no-flow boundary is encountered a natural extension could be done following March et al. (2016) where an additional time scale was applied in an exponential solution overlapping with the analytical

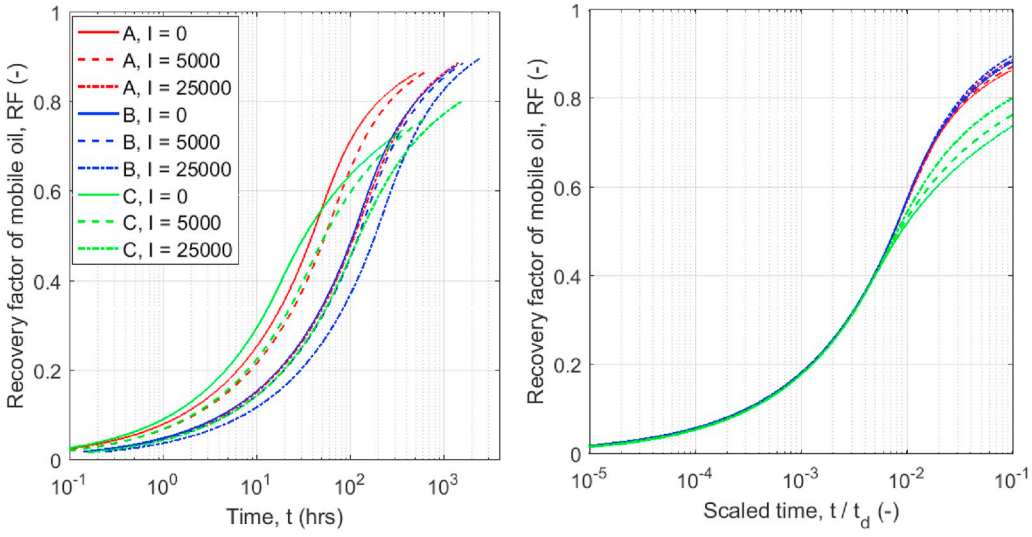

Fig. 9. Recovery factor of mobile oil plotted vs time (left) and scaled time (right) for cases A, B, C (see Table 2) with different fluid-fluid interaction coefficients I (reported in units (Pa s)-1).

solution at the end of the infinite-acting behavior. This is however an approximation of recovery behavior only and does not suggest the development of the in situ saturation profiles.

It can also be mentioned that the analytical solution is valid only under 1D linear flow. Scaling behavior on more general geometries (e.g. core plugs) can be done by replacing the length L with a characteristic length L_C (Shouxiang et al., 1997):

$$L_C = \sqrt{\frac{V_b}{\sum_{i=1}^{n} A_i / l_{A_i}}} \tag{77}$$

where V_b is the sample bulk volume, A_i the area of a given boundary surface, l_{A_i} the distance to its nearest no-flow boundary and n the number of such surfaces. Meng et al. (2019) used dynamical interpolation between two characteristic lengths to improve the geometrical scaling for a 2D system with different boundary conditions. Scaling of the full SI process (until ultimate recovery) often assumes a unique time scale and relatively similar recovery profiles. This can be based on characteristic mobilities Zhou et al. (2002); Standnes and Andersen (2017) or averaging the capillary diffusion coefficient. The variation in scaled profiles due to geometry and late vs early time regimes is often considered negligible compared to unscaled variations where geometrical dimensions, capillary forces and fluid mobilities have the main focus.

5. Discussion

The viscous coupling mechanism is often overlooked in modelling and prediction of multiphase flow processes although derivations from momentum equations indicate that friction between fluids flowing simultaneously can have an impact. Most simulation approaches rely on the extended Darcy model where the relative permeability approach Muskat et al. (1937) is used. Our results show that even if generalized modelling tools are not available, viscous coupling can be accounted for since the generalized model reduces to the conventional relative permeability formulation if a dominant co-current or counter-current flow regime can be assumed.

Even with significant viscous coupling; as long as we have co-current flow it makes sense to apply the co-current relative permeability formulation and if the viscosities are the same the formulas are identical under measured and predicted conditions. The same is true for counter-current flow although these relative permeabilities are more difficult to measure. On the other hand, our simulations have demonstrated that if flow conditions being predicted are not the same as used when measuring relative permeabilities in the laboratory, viscous coupling can lead to significant differences between predicted and true behavior. Viscous coupling is not directly measured during most experimental programs and is implicitly incorporated into the effective output. This underlines the importance of measuring relative permeabilities at representative conditions. Missing quantification of the viscous coupling is partly because a unique parameterization of a generalized model is challenging, perhaps especially under counter-current conditions. Experimental conditions and workflows should be planned carefully to measure functional relations of generalized mobilities as function of saturation and viscosities. If viscous coupling is negligible, viscosity or flow direction will not affect the relative permeabilities, while otherwise it will have an effect. Darcy approach assumptions are consistent with the former behavior, but the presented derivation from momentum equations in this work illustrates that one should be open for the possibility that such a dependence exists.

In this work we demonstrated that counter-current relative permeabilities could be derived under zero net flux conditions. It was shown that these functions always were reduced compared to co-current relative permeabilities derived under equal and same direction phase pressure gradient conditions, even at the end points, but remained non-negative. Previous works Standnes et al. (2017); Qiao et al. (2018); Andersen et al. (2019a) derived counter-current relative permeabilities under equal, but opposite directed phase pressure gradients. The curves derived under those conditions were shown to become negative at low saturations since a strong momentum transfer could lead a phase to travel in opposite direction of what its pressure gradient would suggest. Also, those conditions implied no change in the end points if the same modelling assumptions as here were applied. Standnes et al. (2017) also assumed that the fluid-fluid interaction term depended on the absolute saturations and not the normalized saturations (as used for the fluid-rock terms). The relative permeability end points were still equal between flow modes, but depended on the viscosity of the immobile phase and the fluid-fluid interaction coefficient (as also obtained here for counter-current flow), but specifically depending on the residual saturation indicating how much interface between the fluids there would be to interact. Wang et al. (2006) observed experimental trends that could suggest viscosity has impact on relative permeability end points. Standnes and Andersen (2017) also showed that viscous coupling could account for systematic trends in SI time scales with viscosity not captured by standard models.

In addition to strictly co- or counter-current flow regimes, there are many cases where forced displacement can be significantly affected by capillary forces such as in core flooding (Geffen et al., 1951; Richardson et al., 1952; Andersen et al., 2019b). Assuming that the injection rate $\propto \frac{1}{\sqrt{t}}$, Wang and Sheng (2018) derived analytically that $x(s_w) \propto G'(s_w)\sqrt{t}$ where G is a function that converges to f_w in advection dominated cases and F in capillary dominated cases. This particular flow regime could be a case where the generalized model could be represented using conventional approaches with generalized relative permeabilities.

The role of viscous coupling depends on the flow mode and how conditions change from the reference state. Viscous coupling limits how easily fluids can travel past each other. During co-current flow that was seen by relative permeabilities being adjusted to produce a straight line fractional flow function as viscous coupling increased, indicating that both fluids travel as a single mixture with same speed. For displacement of oil the viscous coupling effect appears to result in more favorable displacement of oil by water flooding. If the viscous coupling in the reservoir is strong in the reservoir than in the laboratory, more favorable displacement can take place, and vice versa. For counter-current displacement stronger viscous coupling generally reduced the imbibition rate. The impact of flow regime is reflected in lower relative permeabilities when switching from co-to counter-current flow. Hence, application of relative permeabilities to model SI processes should be quality checked and adapted to experimental data.

6. Conclusions

Under co-current or counter-current flow conditions have shown that generalized models effectively can be reduced to conventional models using flow regime-dependent relative permeabilities, so-called generalized relative permeabilities. In this work we have extended previous formulations of generalized relative permeabilities to cover counter-current relative permeabilities based on zero net flux, which is representative of counter-current spontaneous imbibition setups. The counter-current relative permeabilities were compared with previously derived co-current relative permeabilities. The relative permeability expressions can be used to construct functions representing the behavior of a generalized model if the flow mode is strictly co- or counter-current and can transfer curves from one flow mode to the other. It was shown that:

- When viscous coupling is accounted for, the counter-current relative permeabilities are always lower than the co-current relative permeabilities, and nonnegative. Especially, the end points are also reduced depending on fluid viscosities and strength of fluid-fluid interaction. In comparison, relative permeabilities derived under

equal, but opposite pressure gradients were in Standnes et al. (2017) found to have negative values for low saturations and equal end points as the co-current relative permeabilities.
- Both oil and water relative permeabilities were reduced by the same saturation dependent coefficient when the flow was changed from co-to counter-current. That result does not depend on the specific generalized model we have used, but appears to depend on the assumed equality of the cross-term mobilities (Onsager's relation).

The generalized relative permeabilities were implemented into analytical solutions relevant for the flow regimes they were valid for. Hence, analytical solutions for forced and spontaneous imbibition were presented that account for viscous coupling. It was seen that:

- Viscous coupling contributes to reduce velocity differences between the fluids. During forced imbibition stronger viscous coupling leads to more favorable oil displacement. During spontaneous imbibition, stronger viscous coupling leads to lower imbibition rate.
- The analytical model for SI was derived for a semi-infinite medium, but validated by comparison with a numerical model with closed inner boundary. The solutions were identical until the no-flow boundary was met.
- A universal scaling was developed for SI that accounts for viscous coupling and arbitrary generalized model input parameters. Recovery factor results scaled with this solution overlap on a square root of time curve until no-flow boundary conditions occur.

Acknowledgments

The authors acknowledge the Research Council of Norway and the industry partners, ConocoPhillips Skandinavia AS, Aker BP ASA, Vår Energi AS, Equinor ASA, Neptune Energy Norge AS, Lundin Norway AS, Halliburton AS, Schlumberger Norge AS, and Wintershall DEA, of The National IOR Centre of Norway for support.

Nomenclature

a_1, a_2, c, k_1, k_2	Correlation parameters for J-function, -
A	Inflow parameter for spontaneous imbibition, m/s^0.5
C_i	Ratio of counter-to co-current relative permeability, -
D	Capillary diffusion coefficient (m^2/s)
f_w	Water fractional flow function, -
F	Fractional flow function for capillary flow
I	Oil/water interaction parameter (Pa·s)$^{-1}$
I_o	Oil/solid interaction parameter, -
I_w	Water/solid interaction parameter, -
J	Leverett J-function, -
k	Absolute permeability, m^2
k_{ri}	Relative permeability
k_{ri}^{max}	Relative permeability end point
$\widehat{k}_{ri}^{co}$	Generalized co-current relative permeability for phase, -
$\widehat{k}_{ri}^{cou}$	Generalized counter-current relative permeability, -
x	Spatial coordinate along reservoir/core (m)
L,	System length, m
n_i	Phase Corey exponent, -
p_c	Capillary pressure, Pa
p_i	Phase pressure, Pa
$Q_w(t)$	Cumulative 1D volume of water imbibed (m)
RF	Oil recovery, -
R	Oil/water interaction term (Pa·s/m^2)
R_o	Oil/solid interaction term, Pa·s/m^2
R_w	Water/solid interaction term, Pa·s/m^2
s_{eq}	Water saturation where $p_c = 0$, -
S_f	Normalized water front saturation, -
s_i	Phase saturation, -
S_i	Normalized phase saturation, -
s_{ir}	Phase residual saturation, -
s_{wc}	Connate water saturation, -
t	Time, s
t^*	Time when imbibition front reaches boundary, s
u_i	Phase Darcy velocity, m/s
u_T	Total Darcy velocity, m/s
u_{w0}	Water flux at inlet during spontaneous imbibition, m/s
v_i	Phase interstitial velocity, m/s
W	Generalized mobility term for capillary diffusion (m^2/(Pa·s))

Greek

α	Water-solid interaction saturation exponent, -
β	Oil-solid interaction saturation exponent, -

θ	Contact angle, rad
λ_i	Phase mobility $m^2/(Pa \cdot s)$
$\widehat{\lambda}_i$	Generalized phase mobility, $m^2/(Pa \cdot s)$
$\widehat{\lambda}_{ii}$	Generalized diagonal mobilities, $m^2/(Pa \cdot s)$
$\widehat{\lambda}_{ow}$	Generalized cross-term mobility, $m^2/(Pa \cdot s)$
$\widehat{\lambda}_T$	Generalized total mobility, $m^2/(Pa \cdot s)$
λ_T	Total mobility, $im^2/(Pa \cdot s)$
μ_i	Phase viscosity, Pa·s
σ_{ow}	Interfacial tension, N/m
φ	Porosity, -
φ_e	Effective porosity, -

Indices

co	Co-current
cou	Counter-current
i	Phase index
o	Oil
w	Water

References

Ambrosi, D., Preziosi, L., 2002. On the closure of mass balance models for tumor growth. Math. Model. Methods Appl. Sci. 12 (05), 737–754.
Andersen, P.Ø., 2019. A simplified modelling approach for petroleum recovery by spontaneous imbibition in naturally fractured reservoirs. J. Nat. Gas Sci. Eng. 63, 95–114.
Andersen, P.Ø., Qiao, Y., Standnes, D.C., Evje, S., 2019. Cocurrent spontaneous imbibition in porous media with the dynamics of viscous coupling and capillary backpressure. SPE J. 24 (01), 158–177.
Andersen, P.Ø., Skjæveland, S.M., Standnes, D.C., 2017. A novel bounded capillary pressure correlation with application to both mixed and strongly wetted porous media. In: Abu Dhabi International Petroleum Exhibition & Conference. Society of Petroleum Engineers.
Andersen, P.Ø., Standnes, D.C., Skjæveland, S.M., 2017. Waterflooding oil-saturated core samples-analytical solutions for steady-state capillary end effects and correction of residual saturation. J. Pet. Sci. Eng. 157, 364–379.
Andersen, P.Ø., Walrond, K., Nainggolan, C., Pulido, E., Askarinezhad, R., 2019. Simulation Interpretation of Capillary Pressure and Relative Permeability from Waterflooding Laboratory Experiments in Preferentially Oil-Wet Porous Media. SPE Reservoir Evaluation and Engineering.
Armstrong, R.T., McClure, J., Berill, M., Rücker, M., Schlüter, S., Berg, S., 2017. Flow regimes during immiscible displacement. Petrophysics 58 (01), 10–18.
Babchin, A., Yuan, J., Nasr, T., 1998. Generalized phase mobilities in gravity drainage processes. In: Annual Technical Meeting. Petroleum Society of Canada.
Bear, J., 2013. Dynamics of Fluids in Porous Media. Courier Corporation.
Bentsen, R., Manai, A., 1992. Measurement of cocurrent and countercurrent relative permeability curves using the steady-state method. AOSTRA J. Res. 7, 169–181.
Bourbiaux, B.J., Kalaydjian, F.J., 1990. Experimental study of cocurrent and countercurrent flows in natural porous media. SPE Reserv. Eng. 5 (03), 361–368.
Brooks, R., Corey, A., 1964. Hydraulic Properties of Porous Media. Colorado State University. Hydrology Papers, No. 3.
Buckley, S.E., Leverett, M.C., 1942. Mechanism of fluid displacement in sands. Trans. AIME 146 (01), 107–116.
Corey, A.T., et al., 1954. The interrelation between gas and oil relative permeabilities. Prod. Mon. 19 (1), 38–41.
Darcy, H.P.G., 1856. Les Fontaines publiques de la ville de Dijon. Exposition et application des principes à suivre et des formules à employer dans les questions de distribution d'eau, etc. V. Dalamont, Paris.
Dullien, F., Dong, M., 1996. Experimental determination of the flow transport coefficients in the coupled equations of two-phase flow in porous media. Transp. Porous Media 25 (1), 97–120.
Ehrlich, R., 1993. Viscous coupling in two-phase flow in porous media and its effect on relative permeabilities. Transp. Porous Media 11 (3), 201–218.
Geffen, T., Owens, W.W., Parrish, D., Morse, R., 1951. Experimental investigation of factors affecting laboratory relative permeability measurements. J. Pet. Technol. 3 (04), 99–110.
Karimaie, H., Torsæter, O., Esfahani, M., Dadashpour, M., Hashemi, S., 2006. Experimental investigation of oil recovery during water imbibition. J. Pet. Sci. Eng. 52 (1–4), 297–304.
Lefebvre du Prey, E., 1973. Factors affecting liquid-liquid relative permeabilities of a consolidated porous medium. Soc. Pet. Eng. J. 13 (01), 39–47.
Leverett, M., 1941. Capillary behavior in porous solids. Trans. AIME 142 (01), 152–169.
March, R., Doster, F., Geiger, S., 2016. Accurate early-time and late-time modeling of countercurrent spontaneous imbibition. Water Resour. Res. 52 (8), 6263–6276.
Mason, G., Morrow, N.R., 2013. Developments in spontaneous imbibition and possibilities for future work. J. Pet. Sci. Eng. 110, 268–293.
McWhorter, D.B., Sunada, D.K., 1990. Exact integral solutions for two-phase flow. Water Resour. Res. 26 (3), 399–413.
Meng, Q., Cai, J., Wang, J., et al., 2019. Scaling of countercurrent imbibition in 2d matrix blocks with different boundary conditions. SPE J. 24 (3), 1179–1191.
Muskat, M., Wyckoff, R., Botset, H., Meres, M., 1937. Flow of gas-liquid mixtures through sands. Trans. AIME 123 (01), 69–96.
Nejad, K.S., Berg, E.A., Ringen, J.K., 2011. Effect of oil viscosity on water/oil relative permeability. In: International Symposium of the Society of Core Analysts. Society of Core Analysts, Austin, TX, USA.
Nooruddin, H.A., Blunt, M.J., 2016. Analytical and numerical investigations of spontaneous imbibition in porous media. Water Resour. Res. 52 (9), 7284–7310.
Odeh, A.S., 1959. Effect of viscosity ratio on relative permeability. Trans. AIME 213, 346–352.
Pooladi-Darvish, M., Firoozabadi, A., 1998. Experiments and modelling of water injection in water-wet fractured porous media. In: Annual Technical Meeting. Petroleum Society of Canada.
Pooladi-Darvish, M., Firoozabadi, A., 2000. Cocurrent and countercurrent imbibition in a water-wet matrix block. SPE J. 5 (01), 3–11.
Preziosi, L., Farina, A., 2002. On Darcy's law for growing porous media. Int. J. Non-Linear Mech. 37 (3), 485–491.
Qiao, Y., Andersen, P., Evje, S., Standnes, D., 2018. A mixture theory approach to model co-and counter-current two-phase flow in porous media accounting for viscous coupling. Adv. Water Resour. 112, 170–188.
Rapoport, L., Leas, W., 1953. Properties of linear waterfloods. J. Pet. Technol. 5 (05), 139–148.
Richardson, J., Kerver, J., Hafford, J., Osoba, J., 1952. Laboratory determination of relative permeability. J. Pet. Technol. 4 (08), 187–196.
Schmid, K., Geiger, S., 2012. Universal scaling of spontaneous imbibition for water-wet systems. Water Resour. Res. 48 (3).
Shouxiang, M., Morrow, N.R., Zhang, X., 1997. Generalized scaling of spontaneous imbibition data for strongly water-wet systems. J. Pet. Sci. Eng. 18 (3–4), 165–178.
Standnes, D.C., 2004. Experimental study of the impact of boundary conditions on oil recovery by co-current and counter-current spontaneous imbibition. Energy Fuels 18 (1), 271–282.
Standnes, D.C., Andersen, P.Ø., 2017. Analysis of the impact of fluid viscosities on the rate of countercurrent spontaneous imbibition. Energy Fuels 31 (7), 6928–6940.
Standnes, D.C., Evje, S., Andersen, P.Ø., 2017. A novel relative permeability model based on mixture theory approach accounting for solid–fluid and fluid–fluid interactions. Transp. Porous Media 119 (3), 707–738.
Wang, J., Dong, M., Asghari, K., 2006. Effect of oil viscosity on heavy oil-water relative permeability curves. In: SPE/DOE Symposium on Improved Oil Recovery. Society of Petroleum Engineers.
Wang, X., Sheng, J.J., 2018. A self-similar analytical solution of spontaneous and forced imbibition in porous media. Adv. Geo-Energy Res. 2 (3), 260–268.
Yuster, S., 1951. Theoretical considerations of multiphase flow in idealized capillary systems. In: Proceedings of the Third World Petroleum Congress, ume 2. E. Brill The Hague, pp. 437–445.
Zhou, D., Jia, L., Kamath, J., Kovscek, A., 2002. Scaling of counter-current imbibition processes in low-permeability porous media. J. Pet. Sci. Eng. 33 (1–3), 61–74.